

THERMAL STABILITY, STRUCTURAL AND OPTICAL PROPERTIES OF RICE HUSK SILICA BOROTELLURITE GLASSES CONTAINING MnO₂

I. ZAITIZILA, M. K. HALIMAH*, F. D. MUHAMMAD, M. S. NURISYA,
M. H. M. ZAID

*Glass and Dielectric Lab, Department of Physics, Faculty of Science, University
Putra Malaysia*

The quaternary glass system $\{[(\text{TeO}_2)_{0.7}(\text{B}_2\text{O}_3)_{0.3}]_{0.8}[\text{SiO}_2]_{0.2}\}_{1-x}\{\text{MnO}_2\}_x$ where $x = 0.00, 0.01, 0.02, 0.03, 0.04$ and 0.05 molar fraction was prepared by melt quenching technique. The amorphous nature of the glass is confirmed by X-ray diffraction patterns and Scanning Electron Microscopy (SEM). The prepared glass samples had also been characterized by Differential Scanning Calorimetry (DSC). The glass transition (T_g), onset glass transition (T_o), crystallization (T_c) and melting temperature (T_m) values were measured from DSC thermo-gram. Results from DSC indicate good thermal stability and low value of fragility (F) of the prepared glass samples. Thermal stability (T_s), Hurby parameter (K_{gl}), fragility (F) and activation energy (E_a) were calculated for every glass composition. It is observed that the optical band gap decreases with the concentration of MnO₂. On the other hand, the refractive index (n) is observed to increase as the concentration of MnO₂ increases. Fourier Transform Infrared (FTIR) spectroscopy has been done to identify the functional group in glass sample.

(Received December 23, 2017; Accepted April 10, 2018)

Keywords: FTIR, UV-Vis, Optical Band Gap, Refractive Index, Differential Scanning Calorimetry

1. Introduction

Recently, tellurite glass has gained significant research interest due to its possibility to be made as a network former because of its various application such as in the field of laser, non-linear applications, optoelectronic and photonics. Tellurite glass shows high refractive index (~ 2.0), low phonon energy (~ 700 cm⁻¹), high dielectric constant, good corrosion resistance and thermal and chemical stability [1-4]. Inorganic borate glasses have been widely used in recent application such as in photonic field.

Borate glasses are advantageous material for radiation dosimetry, infra-red studies, dielectric and insulating materials. Borate glass is usually used in forming system because of its unique and various structural units [5-7]. The pure borate glass contains boroxol ring B₂O₆ that has high bond strength and low cation size. Borate glass also has low refractive index, high melting point and large phonon energy [8].

Silicate glass has high viscosity which can be considered to be used as waveguides in optical communications systems [9]. This silicate glass shows low thermal expansion coefficient, and is chemically durable [10]. Silicate glass is also used as mixed network such as boro-silicate, alumino-silicate, phospho-silicate, sodium-silicate bismuth-silicate glasses or three or more network formers because of its unique ability to infuse into the overall glass structure [11-13].

In this work, silica powder was extracted from the rice husk or rice paddy. Due to the high silica content, rice husk can be processed to extract silicon compounds [14]. Silica extracted from rice husk can reduce disposal problems and can be a cheap raw material rather than buying a commercial silica powder. Main contain of this rice husk contains large amount amorphous silica

*Corresponding author: hmk6360@gmail.com

and other metal impurities such as in a minimum amount. There are many methods to extract silica from the rice husk depending on temperature and duration of burning process [15-17].

The optical, structural and thermal properties of silica borotellurite doped with MnO_2 glass system contain varying concentrations of MnO_2 from 0.00 to 0.05 molar fraction have been studied in this paper. The values of optical band gap energy (E_{opt}) and refractive index (n) are determined to explore the optical behavior of the silica borotellurite glass doped with manganese oxide. Thermal properties of the glass network are measured to investigate the fragility index (F) and activation energy (E_a) of the glass system.

The use of silica from rice husk contribute to a much stronger glass as can be seen in fragility index (F) aside from discovering a new purpose for rice husk waste. About 98.85% of silica were being extracted from the waste utilization of rice husk. No work has been done on optical properties and thermal stability of silica borotellurite doped with manganese.

2. Experimental methods

Glasses with compositional formula $\{[(\text{TeO}_2)_{0.7}(\text{B}_2\text{O}_3)_{0.3}]_{0.8}[\text{SiO}_2]_{0.2}\}_{1-x}\{\text{MnO}_2\}_x$ where $x = 0.00, 0.01, 0.02, 0.03, 0.04$ and 0.05 molar fraction were prepared by melt quenching technique. The glasses were fabricated by mixing thoroughly the chemicals consisting of tellurium (IV) oxide – TeO_2 (Alfa Aesar, 99.99%), boron oxide – B_2O_3 (Alfa Aesar, 98.5%, rice husk ash as silica source – SiO_2 (97.94%) and manganese (IV) oxide – MnO_2 (Alfa Aesar, 99.99%).

Rice husk which was a common agriculture waste was utilized in this project in order to extract silica. The rice husk was washed with distilled water to remove dirt and any other contaminants in the raw material. For the sake of obtaining high purity of silica, the washed rice husk was leached with 2.0 M of hydrochloric acid (HCl) and stirred for 20 minutes. After that, the rice husk was heated at 110 °C for 3 hours. The heated rice husk was rinsed with distilled water in order to get the HCl acid off from rice husk. The rice husk was then dried in an oven at 110 °C for 3 hours. Finally, the rice husk was burned at 600 °C for 6 hours to get white rice husk ash (silica).

The glasses were prepared by mixing all the chemicals in alumina crucible for 30 minutes before being transferred to its first furnace for 1 hour for pre heating at 400 °C. After that, the crucible was transferred to a second furnace and was heated at 1100 °C for 3 hours to aid the melting process. The molten liquid was quenched onto a stainless steel cylindrical shape mould and sent to the first furnace to undergo annealing process for 2 hours at 400 °C. The furnace was then turned off and the sample was left in the furnace overnight to be cooled to room temperature. The rice husk was tested using X-Ray Fluorescence (XRF) spectrometer for elemental analysis.

The X-ray diffractograms were recorded via a PW 3040/60 MPD X'pert high pro analytical (Philips) in the range of $20^\circ \leq \theta \leq 80^\circ$. Optical absorption spectra of all glasses were recorded using UV-Vis spectrophotometer in the spectral range between of 200-800 nm at room temperature. The IR spectra of the glasses were obtained using Perkin Elmer in the range of 280-4000 cm^{-1} . A spectral resolution of FTIR spectroscopy was $\pm 1 \text{ cm}^{-1}$. The thermal characteristic of the glass samples was characterized by differential scanning calorimetry (DSC) at heating rate of 10 °C/min from room temperature to 1200 °C using Thermo Gravimetric Analyzer, (1HT). The microstructure surface of the glass sample was observed by using SEM (LEO 1455 VPSEM) operated at 15 kV and linked with Oxford Inca EDX (energy dispersive X-ray). All the samples were coated with gold using a Bal-Tec coating unit model SCD 005 Sputter Coater.

3. Result and discussion

3.1. XRF analysis

The purity of silica extracted from rice husk in this research was 98.85 %. The purity of the extracted silica depends on the methods of extraction, which includes HCl concentration, burning and leaching temperature. Table 1 unveiled the test result of the purity of extracted silica as well as the percentage of other elements found in the silica that originated from the rice husk.

Table 1. The XRF analyzed result of elements(oxides) and concentrations in white rice husk (silica)

Element (oxide)	Percentage (%)
SiO ₂	98.85
SO ₃	0.75
CaO	0.15
K ₂ O	0.10
Fe ₂ O ₃	0.07
MnO	0.04
ZnO	0.01
CuO	0.03

3.2. XRD studies

X-ray diffraction spectroscopy studies of the silica borotellurite glass were performed at room temperature. Fig. 1 shows the XRD patterns of the glass samples whereby no discrete or continuous sharp peaks can be observed. All XRD patterns exhibit no sharp Bragg's peak indicating amorphous nature of glass system. The only observable hump is indicated by a broad diffuse scattering which can be seen around low angle between 20° and 35° [18-19]. This clearly proves that the glass samples possess amorphous nature without the presence of a long-range atomic arrangement.

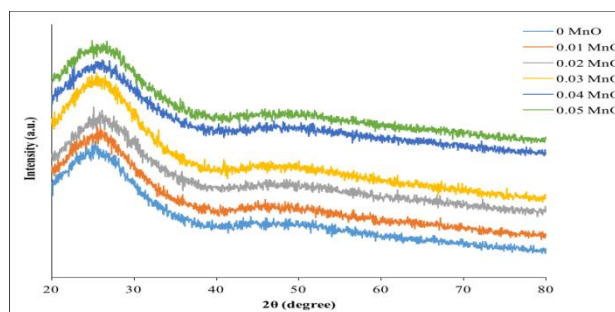


Fig. 1. The XRD for glass sample containing different MnO₂ concentration

3.3. SEM Studies

The SEM micrograph of the glass sample is shown in Fig. 2(a) for the undoped glass and Fig. 2(b) for the glass doped with 0.05 mol fraction of MnO₂. Both SEM images in Fig. 2(a) and 2(b) do not indicate any agglomeration or crystal line occurring in the sample. This proves that the samples are amorphous as confirmed by the XRD pattern. As the concentration of MnO₂ increases, more numbers of micro size grains can be detected, indicating that the glass samples are becoming lighter. It is worth to mention that the prepared glasses are homogeneous without particle aggregate ion. SEM-EDX is a method used to monitor the elements that are present in the glass system. The SEM-EDX spectrum of undoped glass sample is shown in Fig. 3(a) and Fig. 3(b) shows glass sample doped with 0.05 molar fraction of MnO₂. Based on the spectrum in Fig. 3(a), it can be deduced that the elements which exist in the undoped glass consists of B, Si, O and Te. On the other hand, the elements which exists in the doped glass consists of B, Si, O, Te and Mn, as can be seen from the spectrum in Fig. 3(b). In general, the SEM results confirmed that there are no additive impurities in the glass sample. The concentration of every element in the glass sample as obtained from the EDX results for 0% and 0.05% molar fraction of MnO₂ is summarized in Table 2. Based on the table, Te element has the highest concentration since the highest element composition in the glass system is formed by Te.

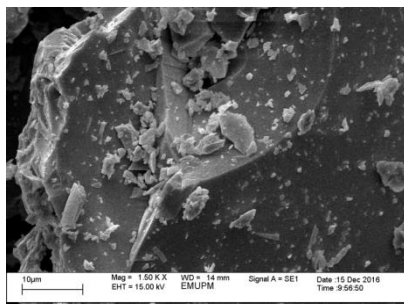


Fig 2. (a) SEM micrograph of undoped silica borotellurite glass

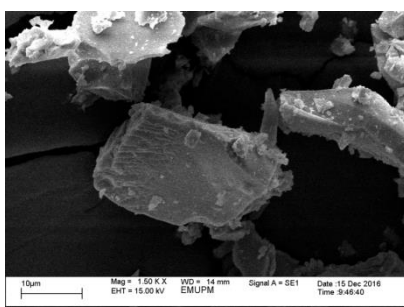


Fig. 2. (b) SEM micrograph of silica borotellurite glass doped with 0.05 mol fraction of MnO_2

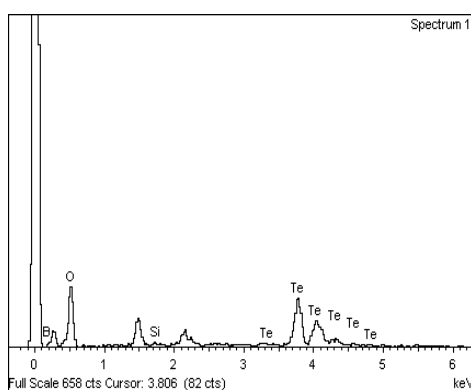


Fig. 3. (a) EDX spectrum of undoped silica borotellurite glass

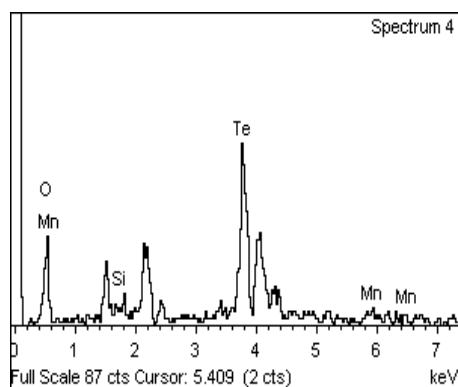


Fig 3. (b) EDX spectrum of silica borotellurite glass doped with 0.05 molar fraction of MnO_2
Table 2. EDX results of undoped and 0.05 molar fraction of MnO_2 in silica borotellurite glass

X (mol %)	Elements				
	B	O	Si	Te	Mn
0	19.93	25.48	0.37	54.21	0
0.05	21.67	25.65	0.44	51.63	0.61

3.4. DSC studies

Differential scanning calorimetry (DSC) is a thermal technique in which the difference in heat flow into a substance and a reference is measured as a function of the sample temperature while the two are subjected to a controlled temperature program [20]. Fig. 4 shows the typical DSC scans at a heating rate of 10 °C/min. DSC curves of all samples are recorded in the range of 0 - 1200 °C. The endothermic hump as revealed by the DSC curves originated from the glass transition whereas the existence of the exothermic peaks in the curves is due to the crystal [21]. The glass transition temperature (T_g), onset crystallization temperature (T_o), crystallization temperature (T_c) and melting temperature were determined from Fig. 4. The obtained thermal parameters are summarized in Table 3.

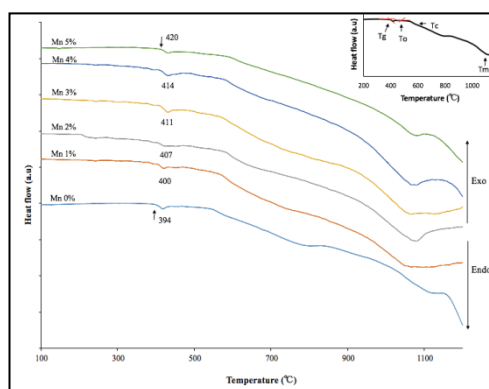


Fig. 4. DSC curves of silica borotellurite glass doped with MnO_2 at heating rate of 10 °C/min

Table 3. Value of glass transition temperature (T_g), onset crystallization temperature (T_o), crystallization temperature (T_c), melting temperature (T_m), thermal stability (T_s), thermal stability (ΔT), Hurby value (K_{gl}), fragility index (F), and activation energy (E_a)

X (mol %)	T_g ($\pm 1^\circ\text{C}$)	T_o ($\pm 1^\circ\text{C}$)	T_c ($\pm 1^\circ\text{C}$)	T_m ($\pm 1^\circ\text{C}$)	T_s ($\pm 1^\circ\text{C}$)	ΔT ($\pm 1^\circ\text{C}$)	K_{gl} (± 0.05)	F (± 0.5)	E_a (± 5) kJ/mol
0	394	495	542	1118	101	12.05	0.26	0.89	11.31
1	400	510	564	1059	110	14.85	0.33	0.88	11.31
2	407	523	578	1081	116	15.68	0.34	0.87	11.31
3	411	530	586	1063	119	16.21	0.37	0.86	11.31
4	414	538	596	1071	124	17.37	0.38	0.86	11.31
5	420	546	606	1078	126	18.00	0.39	0.85	11.31

The T_g values show an increment from 394 °C to 420 °C. The increasing trend in T_g values against the MnO_2 concentration with respect to the increase of the MnO_2 concentration in the rigidity of the glass network as opposed to previous studies in references [22-23]. The change

in T_g clearly shows that the MnO_2 affects the structure of the glass systems. A sample with 0.05 molar fraction of MnO_2 shows the highest stability among all the samples. On the other hand, the undoped glass sample shows the highest T_m . This is probably due to the high concentration of silica whereby the melting point of silica is the highest among all other elements in the glass.

Thermal stability (T_s) of glasses is a measure of disorder of glass network [24]. T_s can be determined by the difference between T_g and T_o values using Dietzel criterion [25], $T_s = T_o - T_g$. A larger T_s value leads to high thermal stability as well as high kinetic resistance of the glass system towards crystallization. In addition, a large value T_s value also retards the nucleation process [26-27]. Another thermal stability (ΔT) equation that is proposed by Saad and Poulin [28] is defined as:

$$\Delta T = \frac{(T_c - T_o)(T_o - T_g)}{T_g} \quad (1)$$

According to the previous research [29] thermal stability is greater when the values of criterion parameters is higher. According to Table 2, sample with 0.05 molar fraction of MnO_2 shows the highest value of ΔT which implies that the sample is most thermally stable. Hruby value (K_{gl}) is a strong indicator of glass forming ability [21,30-31] which is defined as follows:

$$K_{gl} = \frac{T_c - T_g}{T_m - T_c} \quad (2)$$

In this study, the heating rate for all samples was kept constant at 10 °C/min. The K_{gl} value for all samples is found to be more than 0.1 implying that the samples are stable and easy to form a glass [32-33].

Fragility index is a measure of the rate at which the relaxation time decreases with the temperature around T_g using the following relationship [34-36]:

$$F = \frac{E_g}{RT_g \ln 10} \quad (3)$$

where R stands for gas constant, E_g is the activation energy for glass transition which can be calculated using Kissinger formula [37]:

$$\ln\left(\frac{T_g^2}{a}\right) = \frac{E_g}{RT_g} + const. \quad (4)$$

where a is the heating rate of DSC. In this equation, E_g can be calculated from the slope of $\ln(T_g^2/a)$ and $1000/T_g$ as shown in Fig. 5. A linear relationship is observed between the $\ln(T_g^2/a)$ and $1000/T_g$ and the value of E_g for every sample is 11.31 kJ/mol. This is attributed to the similar heating rate of each of the sample.

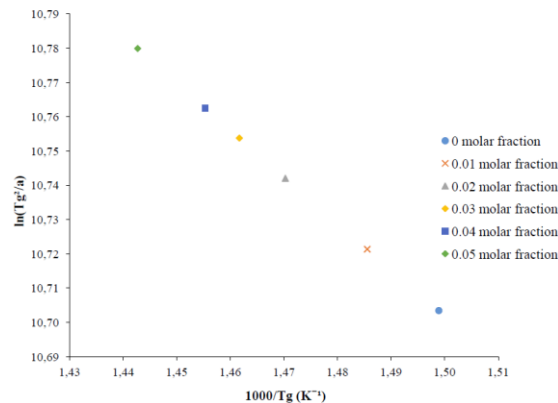


Fig. 5. Plot of $\ln(T_g^2/a)$ vs. $1000/T_g$ (K^{-1}) for silica borotellurite glass doped with MnO_2

The values of fragility index and the activation energy of the glass system are shown in Table 2. Glass forming liquid that exhibits an approximately Arrhenius temperature dependence of the viscosity is defined as strong glass with a low value of F ($F \approx 16$) [38] and the limit for kinetically fragile glass is characterized by a high value of F ($F \approx 200$) [39]. Since the value of fragility index for all glass samples does not exceed 16, the glass samples fabricated can be categorized in the strong glass forming systems.

3.5 Optical spectroscopy

Optical absorption spectra, $\alpha(w)$ of the fabricated samples is determined using the following equation [40-41]:

$$\alpha(w) = 2.303 \frac{A}{d} \quad (5)$$

where A represents the absorbance and d stands for the thickness of the prepared glasses. The relation between $\alpha(w)$ and photon energy, $\hbar w$ is given by the relation [42]:

$$\alpha(w) = \frac{B(\hbar w - E_{opt})^n}{\hbar w} \quad (6)$$

where B is a constant, $n = 1/2$ for direct transition, E_{opt} is the optical band gap energy in eV. In amorphous glass systems, the optical band gap is the energy gap between the valence and conduction band. Equation (6) is employed to calculate the direct and indirect transition that occur in the band gap. The value of indirect E_{opt} can be obtained by extrapolating the absorption coefficient to zero absorption in the plot of $(\alpha \hbar w)^{1/2}$ vs $\hbar w$ shown in Fig 6. [43-45].

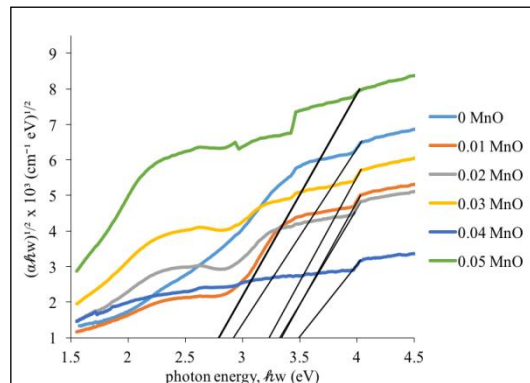


Fig 6. Plot of $(\alpha \hbar w)^{1/2} \times 10^3$ vs. photon energy for silica borotellurite glass doped with MnO_2

The calculated E_{opt} values are summarized in Table 3. These E_{opt} value show a decreasing pattern from 2.72 eV to 2.62 eV as the concentration of the MnO_2 increases. The decrease in the E_{opt} value might be due to the rise of non-bridging oxygen(NBO) as well as the drop of bridging oxygen(BO) number in the glass system. NBO which is more polarizable and bounds an excited electron less tightly than the BO has contributed to the decrement of energy that is essential for an electron to jump from valence band to conduction band. More likely, MnO_2 enters the glass network by breaking up the Te-O-Te and B-O-B bonds and introduces coordinate defect known as dangling bonds along with NBO [32]. The oxygen in MnO_2 will break the local symmetry whereas the Mn^{2+} ions will occupy the interstitial positions. The decrement in E_{opt} value is also due to the increment in BO_3 units at the expense of BO_4 as MnO_2 content increases in the glass system. MnO_2 enters the glass network as a modifier and changes in the structure of the glass system.

However, as in the case of adding 0.01 and 0.04 molar fraction of MnO_2 into the glass system, the E_{opt} value seems to increase. The increasing trend might be the consequence of the role of MnO_2 as a glass former rather than as a glass modifier that creates NBO instead of BO in the

glass system. The rise in amount of BO in the form of TeO_4 in glass samples with 0.01 and 0.04 molar fraction of MnO_2 can be validated via structural studies of the FTIR spectra.

The relationship between the optical band gap (E_{opt}) and refractive index(n) is measured by the relation proposed by Dimitrov and Sakka [46]:

$$\left(\frac{n^2-1}{n^2+2}\right) = 1 - \sqrt{\frac{E_{\text{opt}}}{20}} \quad (7)$$

The calculated values of the refractive index of the glass samples are presented in Table 4.

Table 4. Optical band gap (E_{opt}) and refractive index(n) for silica borotellurite glass doped with MnO_2

Molar fraction MnO_2 (x)	Optical band gap (E_{opt}) (eV)	Refractive index (n)
0	2.72	2.48
0.01	3.17	2.35
0.02	3.14	2.36
0.03	3.06	2.38
0.04	3.25	2.33
0.05	2.62	2.51

The increasing pattern in refractive index as shown in Fig. 7 is attributed to the replacement of TeO^{4+} ions by Mn^{2+} ions which has a lower cation polarizability [47]. Moreover, the increase of the number of high polarizability NBO in the glass system owing to the formation of BO_3 can be verified through the FTIR spectra. The decrease in the refractive index value in 0.02 and 0.04 molar fraction of MnO_2 is due to the dual nature of MnO_2 which acts as modifier and may occupy the network former position [48]. In addition, the decrease of the number of NBO as TeO_4 is formed in the glass system is another factor that may contribute to the decrease of the refractive index values.

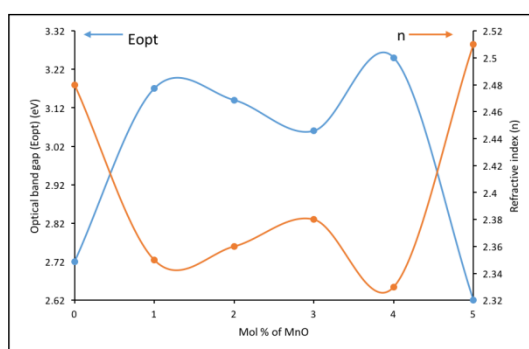


Fig. 7. Optical band gap and refractive index of silica borotellurite glass doped with MnO_2

3.6 FTIR Studies

The effect of doping of MnO_2 on structural properties of $\{[(\text{TeO}_2)_{0.7}(\text{B}_2\text{O}_3)_{0.3}]_{0.8}[\text{SiO}_2]_{0.2}\}_{1-x}\{\text{MnO}_2\}_x$ glass composition has been investigated based on the FTIR spectra obtained from FTIR spectroscopy. FTIR spectra of the prepared glass samples were recorded in the spectral range of $280 \text{ cm}^{-1} - 4000 \text{ cm}^{-1}$ as shown in Fig. 8. The absorption peak in the region of $600 \text{ cm}^{-1} - 656 \text{ cm}^{-1}$ is attributed to the stretching vibration of equatorial and axial Te-O bonds in TeO_4 trigonal bipyramidal unit [47]. It is observed that there is an IR peak in between $671 \text{ cm}^{-1} - 701 \text{ cm}^{-1}$. The

presence of the IR peak in this range is probably due to Te-O vibrations in trigonal pyramid TeO_3 groups [49] and or the presence of B-O-B bridges in various bonding environments [50]. The peak observed around $725\text{cm}^{-1} - 780\text{cm}^{-1}$ in IR spectra is assigned to B-O-B linkages in borate network and bending vibration of bridges containing one trigonal and one tetrahedral boron [51-52]. The intensity of this peak remains almost the same for all glass samples. Another IR peak observed between $801\text{cm}^{-1} - 828\text{cm}^{-1}$ is assigned to B-O bond stretching of tetrahedral BO_4 units [53]. On the other hand, the IR peaks observed between $1079\text{cm}^{-1} - 1124\text{cm}^{-1}$ are assigned to Si-O-Si asymmetric stretching [54]. All studied glass samples have an IR peak between $1232\text{cm}^{-1} - 1243\text{cm}^{-1}$ and the highest intensity at 0.01 molar fraction of MnO_2 . This IR peak is assigned to an asymmetric of relaxation of the B-O bond triangular BO_3 units [53,55]. The band at 1377cm^{-1} to 1382cm^{-1} is assigned to B-O stretching vibrations of BO_3 units in meta-, pyro- and orto- borate group [56-56]. It is found that there is conversion on BO to NBO and vice versa from TeO_4 into TeO_3 and BO_4 to BO_3 . The sample that has the highest absorption intensity is recorded by glass sample with 0.04 molar fraction of MnO_2 . IR peak in the region of $3098 - 3119\text{cm}^{-1}$ is observed in FTIR spectra for 0 and 0.01 molar fraction of MnO_2 which probably corresponds to the fundamental stretching of hydrogen bond [58]. The fundamental groups of Hydrogen bond are observed in the higher region of FTIR spectra. However, the vibration of Mn^{3+} and Mn^{2+} which is around 250cm^{-1} to 380cm^{-1} could not be observed in the IR spectra [50,59-60], probably due to the limitation of the instrument.

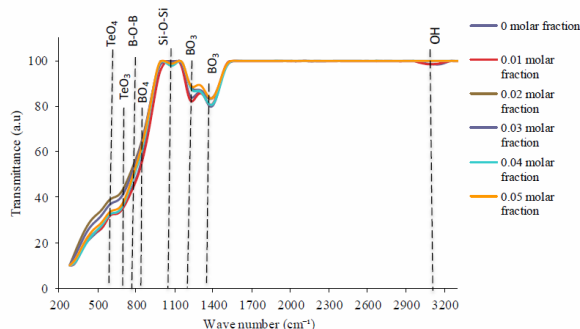


Fig. 8. FTIR spectra of the prepared glass sample with different concentration of MnO_2

4. Conclusion

Silica borotellurite glass doped with manganese with composition $\{[(\text{TeO}_2)_{0.7}(\text{B}_2\text{O}_3)_{0.3}]_{0.8}[\text{SiO}_2]_{0.2}\}_{1-x}\{\text{MnO}_2\}_x$ where $x = 0.00, 0.01, 0.02, 0.03, 0.04$ and 0.05 molar fraction was prepared by melt quenching technique. The XRD measurement of the glass samples exhibits a broad band, proving the amorphous nature of the glass system. The image from SEM measurement shows no crystalline structure which confirms that the glass systems are amorphous. Result from EDX shows no impurities in the glass network. From analysis of DSC, it is found that the prepared glass samples have low value of fragility ($F \approx 16$) and good thermal stability. The IR spectra show that the glass network contains TeO_4 , TeO_3 , BO_4 , BO_3 , Si-O-Si structural units. Optical band gap energy calculated from Mott and Davis formula with respect to the experimentally observed absorption spectra has shown a non-linear behaviour. As the MnO_2 concentration increases, the optical band gap value shows a decreasing trend, which is opposed to the refractive index. This is due to the formation of the NBO that governs linear optical parameters such as optical band gap and refractive index.

Acknowledgments

Authors are thankful to University Putra Malaysia (UPM) through GP-IPS (grant number: 9504400) for providing financial support.

References

- [1] R. A. El-Mallawany, Tellurite glasses handbook: physical properties and data. CRC press. (2011).
- [2] K. Yukimitu, R. C. Oliveira, E. B. Araujo, J. C. S. Moraes, L. H. Avanci, *Thermochimica acta* **426**(1), 157 (2005).
- [3] A. P. Mirgorodsky, T. Merle-Mejean, J. C. Champarnaud, P. Thomas, B. Frit, *Journal of Physics and Chemistry of Solids* **61**(4), 501 (2000).
- [4] S. Rosmawati, H. A. A. Sidek, A. T. Zainal, H. Mohd Zobir, *Journal of Applied Sciences* **8**, 1956 (2008).
- [5] S. M. Abo-naf, *Journal of Non-Crystalline Solids*, **358**(2), 406 (2012).
- [6] E. I. Kamitsos, A. P. Patsis, M. A. Karakassides, G. D. Chryssikos, *Journal of Non-Crystalline Solids*, **126**(1-2), 52 (1990).
- [7] S. Yusub, P.S. Rao, D.K. Rao. *Journal of Alloys and Compound* **663**, 708 (2016).
- [8] R. Reisfeld, *Spectroscopy of Rare Earth Ions*. In *Nanostructured and Advanced Materials for Applications in Sensor, Optoelectronic and Photovoltaic Technology*, A. Vaseashta, D. Dimova Malinovska, J.M. Marshall, Eds.; Springer: The Netherlands 204, 77 (2005),
- [9] P.C. Schultz, *Journal of the American Ceramic Society* **57**(7), 309 (1974).
- [10] Y. K. Sharma, S. S. L. Surana, R. K. Singh, *Indian Journal of Pure and Applied Physics* **46**, 239 (2008).
- [11] M. Szumera, *Spectrochimica Acta Part A: Molecular and Biomolecular Spectroscopy* **129**, 601 (2014).
- [12] B. Mirhadi, B. Mehdikhani, *J. Optoelectron. Adv. Mat.* **13**(9-10), 1309 (2011).
- [13] M. Dult, R. S. Kundu, N. Berwal, R. Punia, N. Kishore, *Journal of Molecular Structure* **1089**, 32 (2015).
- [14] H. Kurama, S. K. Kurama The effect of chemical treatment on the production of active silica from rice husk. In 18th international mining congress and exhibition of Turkey-IMCET. (2003).
- [15] I. S. Mustafa, N. A. N. Razali, A. R. Ibrahim, N. Z. Yahaya, H.M. Kamari From Rice Husk to Transparent Radiation Protection Material. *Jurnal Intelek*, **9**(2) (2015).
- [16] W. Leenakul, T. Tunkasiri, N. Tongsir, K. Pengpat, J. Ruangsuriya, *Materials Science and Engineering C* **61**, 695 (2016).
- [17] T. Lee, R. Othman, F. Y. Yeoh, Development of photoluminescent glass derived from rice husk. *Biomass and bioenergy* **59**, 380 (2013).
- [18] M. H. Wan, M. P. S. Wong, R. Hussin, H. O. Lintang, S. Endud, *Journal of Alloys and Compounds* **595**, 39 (2014).
- [19] M. A. Pandarinath, G. Upender, K. N. Rao, D. S. Babu, *Journal of Non-Crystalline Solids* **433**, 60 (2016).
- [20] D. A. Skoog, F. J. Holler, S. R. Crouch. *Principles of Instrumental Analysis Sixth Edition*. (1998).
- [21] C. Joshi, Y. Dwivedi, S. B. Rai, *Ceramic International* **37**(7), 2603 (2011).
- [22] T. Satyanarayana, M. A. Valente, G. Nagarjuna, N. Veeraiah, *Journal of Physics and Chemistry of Solids* **74**(2), 229 (2013).
- [23] M. Pal, B. Roy, M. Pal, *Journal of Modern Physics*, **2**(09), 1062 (2011).
- [24] I. Soltani, S. Hraiech, K. Horchani-Naifer, H. Elhouichet, B. Gelloz, M. Férid, *Journal of Alloys and Compounds* **686**, 556 (2016).
- [25] Dietzel. *Glass Structure and Properties*. *Glasstech. Ber.* **22**, 1187 (1968).
- [26] O. A. Lafi, M. M. Imran, K. A. Abdullah, *Physica B: Condensed Matter* **395**(1) 69 (2007).
- [27] A. Badaoui, M. Belhadji, *Physical Review & Research International* **3**(4), 416 (2013).
- [28] M. Saad, M. Poulin, *Glass Forming Ability Criterion*. In *Materials Science Forum* (Vol. 19, pp. 11-18). Trans Tech Publications (1987).
- [29] E. R. Shaaban, I. S. Yahia, M. Fadel, *Journal of Alloys Compounds* **469**(1) 427 (2009).
- [30] A. Hrubý, *Czechoslovak Journal of Physics*, **22**(11) 1187 (1972).
- [31] A. A. Joraid, S. N. Alamri, A. A. Abu-Sehly, M. Benganem, *Journal of Non-Crystalline Solids* **358** (10), 1268 (2012).

- [32] S. A. Fayek, M. Fadel, *Journal of Non-Oxide Glasses* **1**, 239 (2009).
- [33] G. S. Murugan, Y. Ohishi, *Journal of non-crystalline solids*, **341**(1), 86 (2004).
- [34] P. Pascuta, M. Bosca, G. Borodi, E. Culea., *Journal of Alloys and Compounds* **509**(11), 4314 (2011).
- [35] A. T. Patel, A. Pratap, *Journal of thermal analysis and calorimetry*, **110**(2), 567 (2012).
- [36] V. Kumar, S. Sharma, O. P. Pandey, K. Singh, *Solid State Ionics* **181**(1), 79 (2010).
- [37] H. E. Kissinger, *Reaction Kinetics in Differential Thermal Analysis*. *Analytical Chemistry* **29**(11) 1702 (1957).
- [38] T. A. Vilgis, *Physical Review B*, **47**(5) 2882 (1993).
- [39] R. Böhmer, C. A. Angell, Local and global relaxations in glass forming materials. In *Disorder effects on relaxational processes* (pp. 11-54). Springer Berlin Heidelberg. (1994).
- [40] M. F. Faznny, M. K. Halimah, M. N. Azlan, *Journal of Optoelectronics and Biomedical Materials* **8**(2), 49 (2016).
- [41] S. S. Hajer, M. K. Halimah, Z. Azmi, M. N. Azlan, *Chalcogenide Letters*, **11**(11) 553 (2014).
- [42] E. A. Davis, N. Mott, *Philosophical Magazine*, **22**(179), 0903 (1970).
- [43] J. Tauc, *Materials Research Bulletin*, **5**(8) 721 (1970).
- [44] N. Elkhoshkhany, R. El-Mallawany, *Ceramics International*, **41**(3) 3561 (2015).
- [45] I. S. Mustafa, H. M. Kamari, W. M. D. W. Yusoff, S. A. Aziz, A. A. Rahman, *International journal of molecular sciences* **14**(2), 3201 (2013).
- [46] V. Dimitrov, S. Sakka, *Journal of applied physics* **79**(3), 1741 (1996).
- [47] P. Gayathri Pavani, K. Sadhana, V. C. Mouli. *Optical, Physica B: Condensed Matter* **406**(6), 1242 (2011).
- [48] M. Ganguli, M. H. Bhat, K. J. Rao, *Solid State Ionics*, **122**(1), 23 (1999).
- [49] O. Ravi, C. M. Reddy, L. Manoj, B. D. P. Raju, *Journal of Molecular Structure* **1029**, 53 (2012).
- [50] D. Möncke, D. Ehrh, E.I. Kamitsos, *Physics and Chemistry of Glasses-European Journal of Glass Science and Technology Part B* **54**(1), 42 (2013).
- [51] I. Ardelean, F. Ciorcas, M. Peteanu, I. Bratu, V. Ioncu, *Modern Physics Letters B* **14**(17-18), 653 (2000).
- [52] E. I. Kamitsos., M. A. Karakassides, G. D. Chryssikos, *Journal of Physical Chemistry* **91**(5), 1073 (1987).
- [53] I. Kashif., A. A. Soliman, E. M. Sakr, A. Ratep, *Spectrochimica Acta Part A: Molecular and Biomolecular Spectroscopy* **113**, 15 (2013).
- [54] C. T. Kirk, *Physical Review B* **38**(2), 1255 (1988).
- [55] B. Karthikeyan, C. S. Suchand Sandeep, J. Cha, H. Takebe, R. Philip, S. Mohan, *Journal of Applied Physics* **103**(10), 103509 (2008).
- [56] M. Todera, S. Filip, I. Ardelean, *Journal of optoelectronics and advanced materials* **8**(3), 1121 (2006).
- [57] I. Ardelean, P. Pășcuță, *Modern Physics Letters B* **16**(14), 539 (2002).
- [58] Z. A. S. Mahraz, M. R. Sahar, S. K. Ghoshal, M. R. Dousti, *Journal of Luminescence* **144**, 139 (2013).
- [59] D Möncke, E. I. Kamitsos, D. Palles, R. Limbach, A. Winterstein-Beckmann, T. Honma, Z. Yao, T. Rouxel, L. Wondraczek *The Journal of Chemical Physics* **145**(12), 124501. (2016).
- [60] A. Winterstein-Beckmann, D. Möncke, D. Palles, E.I. Kamitsos, L. Wondraczek, *Journal of Non-Crystalline Solids* **376**, 165 (2013).